Cryogenics 152 (2025) 104206

Contents lists available at ScienceDirect

Cryogenics

journal homepage: www.elsevier.com/locate/cryogenics

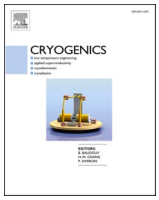

Experimental studies on indirect cooling for a hybrid power transfer line (LH_2 and HTS)☆

Mira Wehr, Michael J. Wolf, Tabea Arndt

Institute for Technical Physics (ITEP), Karlsruhe Institute of Technology (KIT), PO Box 3640, 76021 Karlsruhe, Germany

A B S T R A C T

This contribution presents conceptual designs for a hybrid power transfer line (PTL) with liquid hydrogen (LH_2) and high temperature superconductors (HTS). The synergetic combination of chemical and electrical energy transfer provides a high overall efficiency and large power density. To avoid critical material compatibility with hydrogen and improve safety aspects, one option is to place the HTS cable within the same cryostat but separated from the LH_2 flow by a protective pipe. A key challenge of this indirect cooling is the heat transfer capability from the cable to the hydrogen. To improve the thermal contact, the protective pipe is filled with helium as a contact gas. Evaluating the indirect cooling needs modelling of heat transfer by natural convection, which relies on empirical correlations. In this work, an experiment is designed to validate the correlations at cryogenic temperatures. The presented test set-up is of reduced geometric complexity and experiments are executed with liquid nitrogen (LN_2) at 77 K. The measurement series includes different cable sample topologies and the overall results show a good accordance with a chosen empiric description of natural convection in enclosed space. The outcome enables further quantitative investigations of the indirect cooling concept for hybrid PTLs. Preliminary results predict a sufficient thermal coupling between the HTS cable and stagnant helium.

1. Introduction

The decarbonization of the energy sector needs large-scale green energy carriers since transport and distribution are crucial.

Hydrogen, when produced by electrolysis with electricity gained from renewable energy sources, has a great potential to fill this need. Among many forms of its transportation, the liquid state has significant advantages. When cooled down to $20K$, hydrogen possesses high gravimetric and volumetric power densities ($118.12MJkg^{-1}$ and $8403.3MJm^{-3}$ at ambient pressure, respectively) as well as great coolant properties with a heat capacity of $9.57kJ(kgK)^{-1}$ [1]. The downside, however, is an energy-costly liquefaction process with high losses.

Another green energy vector is renewably produced electricity itself. Superconducting cables for high current transmission show high electrical power densities and therefore require less resources in terms of material and space. Yet they need a considerable cooling effort to operate at cryogenic temperatures. The advantages of a synergetic combination with LH_2 transport are therefore obvious.

The idea to combine liquid hydrogen and superconductors to yield large scale power transfer by chemical and electrical energy is not new. In 2004, [2] proposed the idea of a "SuperCable" with dual delivery of hydrogen and electric power, yet his following works to the subject (e.g. [3,4]) remained theoretical. A first attempt at an experimental proof-of-concept for an LH_2 cooled superconducting power cable was successfully conducted by [5] in 2011 and further developed in the following years [6–8]. The authors used magnesium diboride (MgB_2) based superconducting wires in a flexible LH_2 line. However, the use of commercially available HTS based on rare earth barium cuprate (REBCO) tapes at a LH_2 temperature level of around 20——30 K offers unique benefits in terms of performance and stable operation over a wider temperature range (e.g. YBCO: $I_c/w(T = 20K) > 4000Acm^{-1}$, [9]). Furthermore, a rigid pipeline with smooth hydraulic surfaces instead of a corrugated pipe to keep flexibility will greatly reduce the pressure drop of the LH_2 flow [10]. The design will also be easier to adjust to greater mass flows. This work will therefore explore an alternative design.

2. Hybrid pipeline – Conceptual designs

The hybrid power transfer line consists of a thermally insulated rigid pipeline (vacuum and Multi-layer insulation MLI) for LH_2 transportation, and a compact electric superconducting cable that is placed in the same cryostat and thermally coupled to the cryogen. The direct current (DC) cable is designed as biphasic and concentric, with included electrical insulation between the phases and to the environment. Because of its excellent performance at LH_2 temperatures, the 2G HTS material YBCO is used.

In the following, two basic conceptual hybrid pipeline designs are introduced.

☆ This article is part of a special issue entitled: 'HTS Cooling 2024' published in Cryogenics.

https://doi.org/10.1016/j.cryogenics.2025.104206
Received 20 December 2024; Received in revised form 12 August 2025; Accepted 26 September 2025
Available online 27 September 2025

2.1. Direct cooling

The direct cooling concept follows a superconducting cable topology that has widely been realized for different cryogens including liquid nitrogen and hydrogen (e.g. [5–8,11]). To optimize convective cooling by forced flow, the wires are in direct contact with the liquid cryogen. Fig. 1 shows an exemplary scheme of an LH_2 cooled cable with main components. For an optimized thermal coupling to the inner layers of superconductor as well, the flow cross-section is often divided in a circular channel inside of the cable and an annular gap on the outside (see for example [5]).

Since the cables usually consist of many layers of different materials (e.g. copper former, electrical insulation, wound superconductor and support tapes), the integral structure is porous allowing the fluid to penetrate. As a result, the cable is thermally coupled by high heat transfer coefficients outside and inside and shows a high effective thermal diffusivity in the cross section [5].

2.2. Indirect cooling

For LH_2-cooled cables, additional circumstances have to be considered. Hydrogen is known to lead to embrittlement and material fatigue in some materials [12]. While austenitic stainless steel has been shown to endure cryogenic hydrogen environments [13], the hydrogenation of the REBCO ceramic layer of 2G HTS at high temperatures $> 450K$ has a degrading effect on the superconducting properties [14]. However, the long-term exposure effect on the ceramic layer in LH_2 at cryogenic temperatures is yet unknown. Therefore, to avoid material incompatibilities and increase the safety (e.g. tightening/sealing), the indirect cooling concept (Fig. 2) places the superconducting cable inside a protective stainless-steel pipe as a material barrier against the hydrogen bulk flow. To thermally couple the superconductor to the cryogen, the pipe is filled with a contact gas. At liquid hydrogen temperature level of around $22K$, the only suitable non-flammable gas is helium. Various works have been investigating and testing superconducting cables cooled with gaseous helium e.g. [15–17], they are however generally designed with a flow system for the cryogen to provide the cooling power.

In the here presented configuration, the heat transfer from the cable to the helium is of conductive or natural convective nature, depending on density and temperature gradients. Generally, a much lower transfer coefficient than a forced flow heat transfer is expected. Investigations are needed to evaluate the cooling ability of stagnant helium gas.

Chapter III describes the underlying thermodynamics and convection model.

3. Description of natural convective heat transfer

A challenge of developing a reliable model for heat transfer by natural convection is to determine the heat transfer coefficient between a solid surface and a fluid. It is dependent on substance properties and geometry and can only be obtained from empirical models or measurements. Pertinent literature describes formulas based on characteristic numbers and geometric aspects as used in fluid mechanics. [18] proposes an empirical correlation for the heat transfer rate $\dot{Q}$ by natural convection in enclosed space for a horizontal cylindrical annulus as:

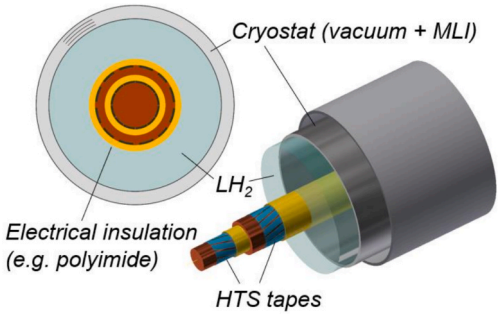

Fig. 1. Scheme of direct cooling design: the cable is placed directly in the LH_2 flow.

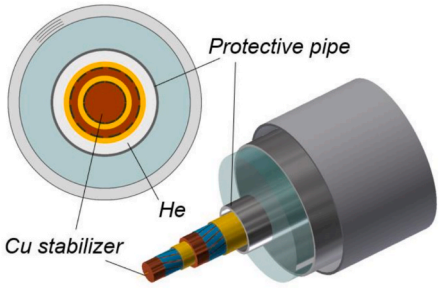

Fig. 2. Scheme of indirect cooling design: the cable is placed in a protective steel pipe filled with helium as a contact gas.

$$\dot{Q} = \frac{2\pi\lambda_{eff}L}{\ln(D_o/D_i)}(T_i - T_o) \tag{1a}$$

where

$$\frac{\lambda_{eff}}{\lambda} = 0.386\left(\frac{Pr}{0.861+Pr}\right)^{1/4}(Ra^*_{cyl})^{1/4} \tag{1b}$$

$$(Ra^*_{cyl})^{1/4} = \frac{\ln(D_o/D_i)}{\delta^{3/4}\left(D_i^{-3/5}+D_o^{-3/5}\right)^{5/4}}Ra_\delta^{1/4} \tag{1c}$$

$$Ra_\delta = \frac{g\beta(T_i - T_o)\delta^3}{\nu^2}\mathrm{Pr} \tag{1d}$$

$$\delta = \frac{1}{2}(D_o - D_i) \tag{1e}$$

The indices o and i indicate the diameters D and surface temperatures T of the outer ('cold') and inner ('hot') cylinder, respectively, and L the cylinder length. The substance properties thermal conductivity λ, viscosity ν, and coefficient of volume expansion β describe the state of the fluid at $T = (T_i + T_o)/2$. In Equation (1d), g is the gravitational acceleration. The dimensionless numbers Rayleigh (Ra) and Prandtl (Pr) describe the character of heat transfer in a fluid and the relation of viscosity to thermal conductivity, respectively. For a more detailed explanation, it is referred to [18] and [19].

The heat transfer coefficient α can then be obtained from [18]

$$\dot{Q} = \alpha A_m(T_i - T_o) \tag{2a}$$

with

$$A_m = \frac{A_o - A_i}{\ln(A_o/A_i)}, \tag{2b}$$

A being the respective surface area. Fig. 3 shows the thermodynamic steady-state energy balance model for convective cooling of a cable in gaseous helium environment.

Neglecting heat loss trough radiation and conduction, it can be assumed that in steady-state conditions the heating power $\dot{Q}_{heat}$ created

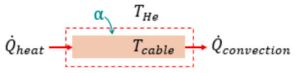

Fig. 3. Energy balance model for convective cooling of the cable in steady-state.

inside the cable equals the convective cooling power $\dot{Q}_{convection}$ over the surface to the gas (see Fig. 3). The basic energy balance then delivers

$$\dot{Q}_{convection} = \alpha A \Delta T = \dot{Q}_{heat} = UI \tag{3}$$

where A describes the area of heat transfer and $\Delta T = T_{cable} - T_{He}$ equals the temperature difference between the cable surface and the bulk gas. Presuming all of the externally applied heating power is electrical (neglecting Joule losses of the wires), α then can be directly obtained from measuring temperature gradients and the known electrical quantities voltage U and current I.

Empirical correlations are only valid for a known range of boundary conditions. The correlation described in Equations (1)-(3) is considered confirmed for Prandtl numbers $1 < Pr < 5000$ [18]. With helium having a Prandtl number of Pr ≈ 0.7 [1], experimental validation of these formulations is necessary.

4. Experiments

4.1. Set-up

The experimental set-up is designed to represent a section of a superconducting cable in a gas-filled protective pipe immersed in the liquid cryogen. Fig. 4 shows the test bench scheme and a photography of a sample during installation.

The cable sample (1) is geometrically reduced to a cylinder, different sample versions will be described in detail below. The heat source is realized by two heating cartridges (2) which are placed in concentric boreholes over the length of the sample. Platinum temperature sensors (Pt100) (3) are used to measure temperatures, details on the positioning of these sensors are given below.

Two types of samples (A, B) are placed coaxially in the protective pipe on 3D-printed PLA spacers (4), which are designed to minimize heat transfer by conduction. These white spacers can easily be identified in the front of the sample's photo in Fig. 4. The protective pipe (5) is made of stainless steel and placed in a liquid nitrogen (LN_2) bath (6) to represent constant cooling at its outer surface. For this experiment, LN_2 provides a safer and more accessible testing environment than LH_2. The pipe can be filled with helium (7) in varied pressures. Helium supply, sensorics, and electrical power for heating can be accessed through vacuum-tight feedthroughs (8, 9).

Table 1 summarizes dimensions and parameters of the experiments.

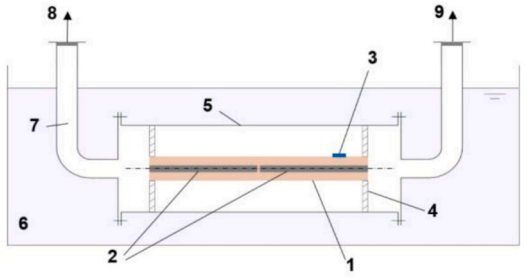

1 Cable sample of reduced geometric complexity
2 Heating cartridges: constant heat source
3 Pt100 temperature sensors
4 3D printed spacers (PLA)
5 Protective pipe (stainless steel)
6 Liquid nitrogen bath (LN_2)
7 He in varied pressures
8 Feedthrough: He supply
9 Feedthrough: sensorics

Fig. 4. Schematics of experimental set-up and photo of a sample during assembly (not to scale, the sensor placement is symbolic. More details in Section B.).

Table 1
Experimental dimensions and parameters.

Diameter of protective pipe	$D = 100mm$
Length of cable sample / Cu rod	$L = 300mm$
Diameter of Cu rod	$d = 20mm$
Thickness of PI (2 layers)	$\delta_{PI} = 2{*}0.15mm = 0.3mm$
He pressures	$p_{He} = 100 \cdots 1,000mbar$
Heating power	$P_{heat} = 0 \cdots 15W$

It is emphasized that the main objective is the validation of an empirical correlation for heat transfer. For natural convection, the most important geometric dimension is the cable diameter which is realistic, others are chosen for feasibility. Likewise, the heating power is exaggerated compared to a realistic heat loss of a superconducting DC cable to cover a broader range of boundary conditions. Fig. 5 shows schematics of the different samples, which are designed to investigate different aspects of the heat transfer in hybrid pipelines separately. In sample A, the cable specimen (1) is geometrically reduced to a bare copper rod and located coaxially inside the steel pipe on 3D-printed spacers (4). The second sample B includes two overlapping layers of polyimide (PI) foil wound around the Cu rod to mimic the influence of the required electrical insulation. In literature, this type of configuration is known as 'cold dielectric'; all samples in this study belong to this category. Sample B is also located coaxially inside the steel pipe using the PLA spacers.

A third sample C places the PI-covered copper rod loosely on the bottom of the steel pipe without spacers, such that it forms a solid–solid contact in line form. The goal of this sample is to investigate the effect of additional conductive cooling on the cable temperatures.

4.2. Sensorics

Temperatures on the cable sample surface are measured with Pt100 resistance sensors that are contacted with epoxy glue. A total of six sensors are placed on the copper rod, distributed randomly over length and circumference to monitor the effect of position. Preliminary tests showed a uniform temperature distribution over the surface. Following measurement values are averaged over the number of sensors. On sample B, five additional sensors are attached to the PI foil (see Fig. 6) and were treated in the same way. [17] proposed that for convection in sufficiently small spaces, the temperatures T_i and T_o from Equation (1a) represent the temperatures of the enclosing solid surfaces instead of the bulk fluid. Therefore, instead of measuring the helium temperature, temperature measurements on solid surfaces are used. For T_o, a Pt100 sensor is glued on the inside of the steel pipe (Fig. 6). Preliminary tests confirmed the assumption that the immersed pipe is in thermal equilibrium with the LN_2 across its length and circumference.

The Pt100 sensors are connected via four-wire measuring with feed current $10\mu A$, using a SCXI-1125 module from National Instruments for data acquisition. The helium pressure is monitored by an analog manometer which is frequently nulled. It is assumed that an approximated cumulated uncertainty of < 3 % is sufficient for the scope of this work.

4.3. Experimental execution

After installation of the sample in the pipe and vacuum-tight closing the flanges, the vessel is evacuated to clear residual gas. Then the vessel is filled with helium at different pressures. The cooldown to LN_2 temperature, although time consuming, is monitored to ensure that all sensors are working and to start from a defined quasi-stationary temperature.

The heating cartridges supply the sample at a defined power until a steady temperature is measured. The procedure is then repeated for different heating powers. To evaluate the experimental results, the measured temperature differences for individual helium pressures and

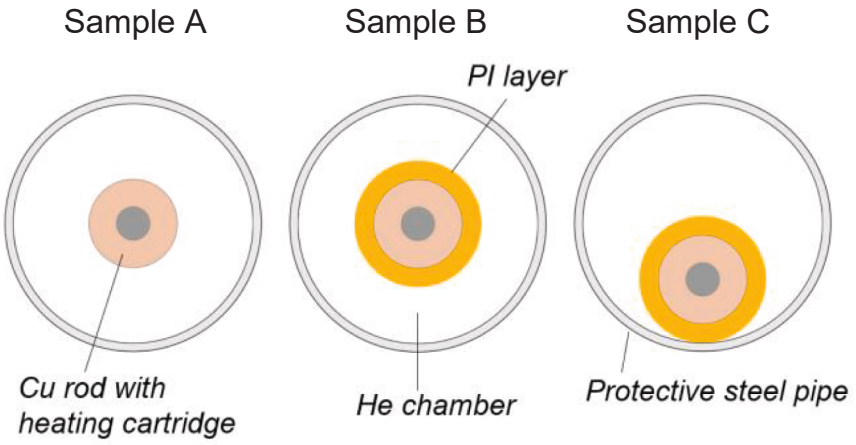

Fig. 5. Schematic cross-sections of different samples (not to scale). A: Cu rod placed coaxially inside the steel pipe; B: Cu rod wrapped in PI foil (2 layers), coaxially inside the steel pipe; C: Cu rod wrapped in PI foil (2 layers), placed on the bottom of the steel pipe.

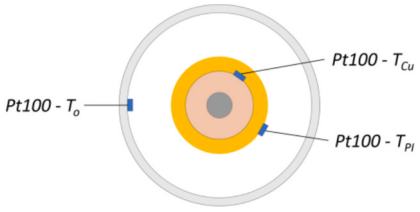

Fig. 6. Schematic sensor placement in cross-section, depicted here is sample B with PI foil wound around the Cu rod.

heating powers are plotted against the empirical predictions. Fig. 7 shows an exemplary cooldown and subsequent heating curve for sample A and a helium pressure of $p_{He} = 1,000 mbar$.

5. Results

Fig. 8 shows the temperature difference ΔT of sample A as a function of the heating power for various helium pressures. As expected, the temperature difference increases with increasing heating power for a given helium pressure. Similarly, the temperature difference decreases with increasing helium pressure for given heating power. Measurements are represented by symbols and the expectation from calculations (Equations (1a)-e) is shown as color-matching solid lines. The chosen correlation from [18] generally matches the measurements. The agreement improves with increasing helium pressure. At the same time, considering a conservative approach neglecting radiation and heat conduction through the spacers, the empirical values consistently predict higher temperature differences between sample surface and gas and thus lower heat transfer coefficients. The calculations will therefore

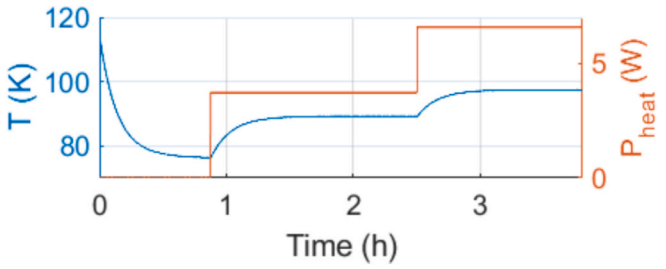

Fig. 7. Exemplary cooldown and heating curve for sample A and $p_{He} = 1,000 mbar$.

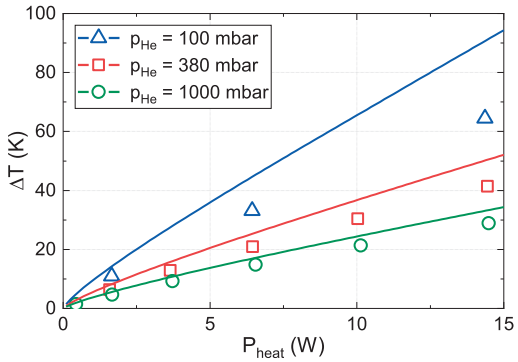

Fig. 8. Comparison of measurements (symbols) and empirical calculations (solid lines) for different He pressures and heating powers.

underestimate the real cooling power and provide an intrinsic safety margin. The assumption of a negligibly small radiation heat transfer of the sample to the steel pipe is considered valid since it is approximated to be smaller than 2 % of the induced electrical power due to the immersion in LN_2 (calculated with an emission grade of $\varepsilon = 0.7$).

Sample B of the experiment repeats the first series with an PI covered rod to measure the insulating effect of a dielectric material with low thermal conductivity ($\lambda_{PI} = 0.1255 W(mK)^{-1}$ at $T = 77K$, [20]). In Fig. 9, the temperature gradients of the temperature sensors on the PI foil of sample B (green circles) are plotted together with data of sample A

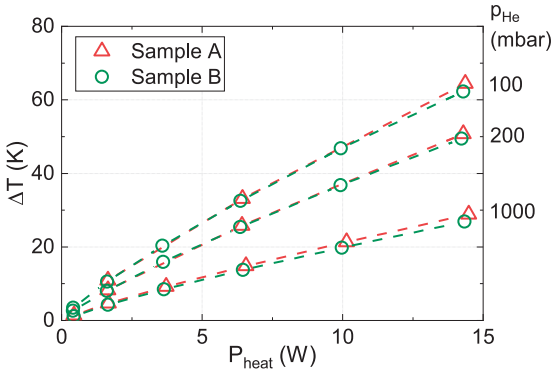

Fig. 9. Comparison of outer surface temperature differences of samples A and B (Cu rod with PI foil). Dashed lines connect data points to guide the eye.

(red triangles) for different helium pressures and heating powers.

The temperature sensors on the PI foil of sample B and on the copper rod of sample A represent in both cases the outermost temperature and therefore the relevant heat transfer surface temperatures for the heat transfer to the helium gas. It can be seen that the temperature differences on the outermost surfaces of both samples match very well for all investigated pressures and heating powers. The results confirm the statement implied in Equations (1a)-e), that the physical mechanism of natural convection is independent from the solid material and type of surface. Therefore, as expected, the measurement points match regardless of the heating power and helium pressure.

In Fig. 10, the temperature differences between the copper surface T_{Cu} under the insulation layer and the outer PI temperature T_{PI} of sample B, $\Delta T = T_{Cu} - T_{PI}$, is plotted as a function of the heating power. Since the agreement with the correlation increases with increasing helium pressure, only $p_{He} = 1,000 mbar$ is considered.

It is observed that the temperature difference increases nearly linearly as a function of the heating power in the considered temperature range. A significant deviation from the measurements can be observed when calculating the expected thermal resistance through the PI layer assuming perfect contact conditions between the outer surface of the copper and the inner surface of the PI ($T_{Cu}(r = 10mm) = T_{PI}(r = 10mm)$) as

$$R_{th,PI} = \frac{\ln((d + \delta_{PI})/d)}{\lambda_{PI} 2\pi L} \tag{4}$$

with d being the copper rod diameter, L its length, and δ_{PI} the thickness of the PI layer. λ_{PI} is the thermal conductivity of PI at the respective temperature.

The resulting theoretical temperature difference is then obtained by

$$\Delta T_{Cu-PI} = P_{heat} R_{th,PI} \tag{5}$$

This dependency is plotted in Fig. 10 for single points (crosses). The dotted black line is shown to guide the eye. The calculations show a significantly smaller temperature dependence compared to the actual measurements.

This difference can be explained by not-perfect contact conditions, leading to an additional thermal contact resistance $R_{th,c}$ which needs to be added to the "perfect, solid-state" thermal resistance $R_{th,PI}$, leading to

$$R_{th,total} = R_{th,PI} + R_{th,c} \tag{6}$$

The thermal contact resistance between two solid layers is specific for a given sample, depending for example on the quality of contacting surfaces, contact pressure, and possible interlayers [21]. For the experiments in this work, the contact resistance between the cable components

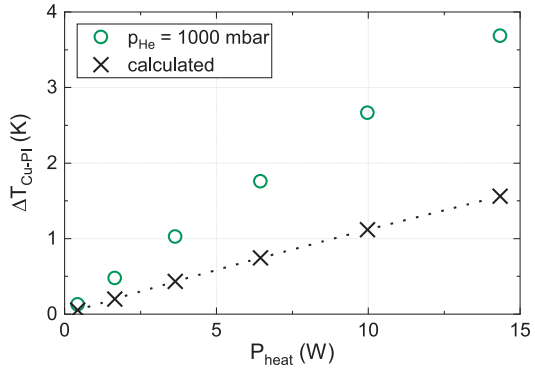

Fig. 10. ΔT between Cu surface and outer PI surface over heating power. The circles show measurement points, whereas the black crosses mark the calculated values assuming perfect contact conditions between the layers. Temperature dependencies of material properties are considered. The dashed line is implemented to guide the eye.

copper and polyimide can be derived from the difference of the measurement data and the calculated values. Table 2 shows $R_{th,c}$ for each measurement point.

The values of the thermal contact resistances decrease slightly with increasing heating power and therefore temperature difference.

In Fig. 11, the influence of a combined conductive and convective heat transfer is investigated with the help of sample C, which is lying on the bottom of the protective pipe. The temperature difference $\Delta T = T_o - T_{PI}$ is plotted as a function of the heating power. Data of sample C (purple color) are compared to the results of B (green color) from Fig. 9 for two different helium pressures, shown in different symbols. As expected, the temperature differences of sample C are always smaller than for sample B due to the additional path for heat transfer. The effect of increased cooling power by additional heat conduction decreases with higher helium densities. Considering the non-optimized solid–solid line contact and altered convection geometry, it is challenging to reliably quantify the effect or derive an experimental value for the thermal contact resistance. Yet the results suggest that the cooling capability by additional heat conduction can be improved by design.

6. Implications for cable design

Considering the empirical correlation for heat transfer by natural convection in enclosed spaces to be sufficiently validated for a cable and pipeline geometry at LN_2 temperature, the findings are now extrapolated to a liquid hydrogen environment to estimate the cooling power of a hybrid energy pipeline design with indirect cooling. The following calculations serve to show the implications of the results in a simplified pipeline model, as sketched in Fig. 12.

The following time-independent, steady-state calculation considers only a single electric phase and that the heating power $P_{heat,Cu}$ is created in the inner copper core of the cable and homogeneous over the cable. For a superconducting cable, this might be due to fault events, e.g. from a resistive current bypass. Starting with the temperature of the LH_2 mass flow, the LH_2 will be heated up following Equation (7), representing a steady-state energy balance (heating through cryostat losses, radiation, and flow dissipation are neglected):

$$\frac{dT_{LH2}}{dx} = \frac{P_{heat,Cu}}{\dot{m}_{LH2} \bar{c}_{p,LH2}}, T_{LH2}(x = 0) = T_{LH2,in} \tag{7}$$

Assuming constant fluid properties as only small temperature increases and pressure drops over the length of the cable sufficiently far from the critical point of H_2 are considered, one expects a linear temperature increase along the pipeline length ($x = L_{PTL}$). The mean heat capacity of liquid hydrogen $\bar{c}_{p,LH2}$ is specified at [1]

$$\overline{T}_{LH2} = \frac{T_{LH2,in} + T_{LH2,out}}{2} \tag{8}$$

$$\overline{p}_{LH2} = \frac{p_{LH2,in} + p_{LH2,out}}{2} \tag{9}$$

with indices $LH2, in$ and $LH2, out$ indicating the pipeline inlet and outlet

Table 2
Thermal contact resistances $R_{th,c}$ between the Cu surface and the PI foil, derived from measurement data and calculated ideal contact conditions.

$P_{heat}(W)$	$R_{th,c}(KW^{-1})$
0.43	0.178
1.65	0.168
3.64	0.163
6.45	0.157
9.97	0.155
14.34	0.148

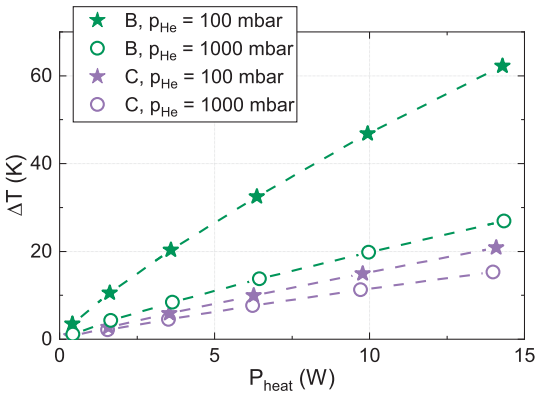

Fig. 11. Comparison of experiments with sample B and C to investigate the effect of increased cooling power by additional conduction.

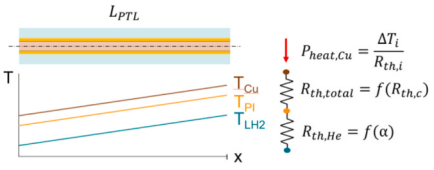

Fig. 12. Reduced thermal model of a hybrid pipeline with respective thermal resistances $R_{th,i}$ derived from measurement data and validated empirical correlations.

temperatures and pressures of the liquid hydrogen flow (see Table 2). The heat transfer from the copper cable through the electrical insulation layer PI and the helium gas to the LH_2 flow is described by thermal resistances $R_{th,i}$ connected in series. The total thermal resistance in the solid layers between the copper and the outer surface of polyimide is calculated from equations (4) and (6), with $R_{th,c}$ being the experimentally obtained contact resistance between copper and PI from Table 1. Since more experiments at lower temperatures are missing, for further investigations a conservative 'worst case' value of $R_{th,c} = 0.2KW^{-1}$ is set and then scaled to $R_{th,c} = 0.06KmW^{-1}$ for calculations referred to $1m$ cable length. The thermal resistance of the helium phase is reduced to the convective heat exchange interface and described as

$$R_{th,He} = \frac{1}{\alpha\pi(d + 2\delta_{PI})} \tag{10}$$

where α is the heat transfer coefficient obtained from the experimentally validated empirical formula with material properties at LH_2 temperature. $R_{th,He}$ is also referred to $1m$.

Overall, this leads to the following maximum temperature of the copper core at $x = L_{PTL}$:

$$T_{Cu,max} = T_{LH2,in} + \frac{P_{heat,Cu}}{\dot{m}_{LH2}\bar{c}_{p,LH2}} L_{PTL} + P_{heat,Cu}\left(R_{th,total} + R_{th,He}\right) \tag{11}$$

For the cable design, a maximum allowed temperature defines the current carrying ability of the superconductor, approximated here as the copper temperature $T_{Cu,max}$. Starting with an initial LH_2 temperature $T_{LH2,in}$ to ensure liquid state, the maximum allowed fluid temperature at the pipeline outlet $T_{LH2,out}$ depends on the pressure (here assumed: $p_{LH2,in}$ and $p_{LH2,out}$ from Table 2). The thermal calculations deliver the needed helium pressure to achieve sufficient cooling. For a given set of parameters (see Table 3.), the results can be shown as a color plot in Fig. 13.

Table 3
Parameters for exemplary cable cooling calculations with a simplified thermal model.

Cable diameter	$d = 20mm$	Inlet T LH_2	$T_{LH2,in} = 22K$
Thickness PI	$\delta_{PI} = 0.3mm$	Inlet p LH_2	$p_{LH2,in} = 6bar$
Pipeline length	$L_{PTL} = 1,000m$	Outlet T LH_2	$T_{LH2,out} < 25K$
Mass flow LH_2	$\dot{m}_{LH2} = 1.66kgs^{-1}$	Outlet p LH_2	$p_{LH2,out} = 4bar$
Heat capacity LH_2 [1]	$\bar{c}_{p,LH2} = 11.66kJ(kgK)^{-1}$	Max. Cu temperature	$T_{Cu,max} < 35K$

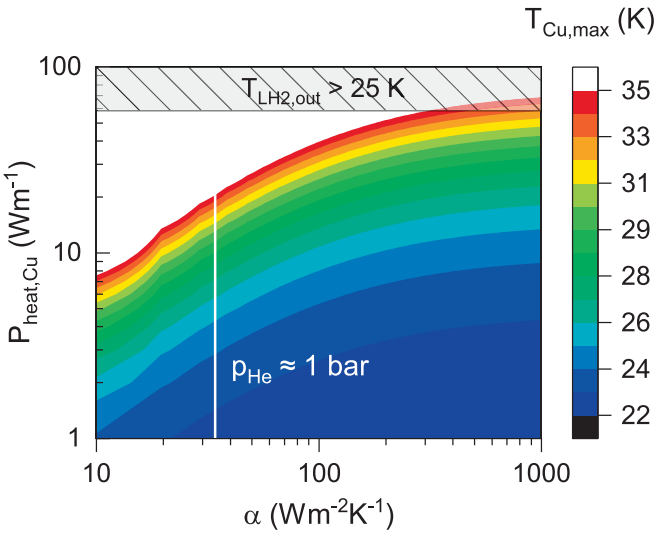

Fig. 13. Depiction of a constant cable cooling power and LH_2 outlet temperature depending on the heat transfer coefficient between the cable surface and the fluid. Example: with $p_{He} = 1bar$ in indirect cooling, α is sufficient to cool up to $P_{heat,Cu} = 20Wm^{-1}$ and not exceed the allowed Cu temperature $T_{Cu,max} = 35K$.

7. Conclusion

This work explored an alternative cooling concept of superconducting cables with LH_2, by placing the cable in a stagnant helium environment to avoid material incompatibilities. The key findings are summarized below:

- For the first time, studies have been conducted on cooling an HTS cable with stagnant helium gas instead of forced flow to simplify the cooling system. The temperature level is provided by liquid hydrogen in a combined hybrid energy pipeline.
- The empiric correlation of natural convective cooling in enclosed spaces by [18] could be sufficiently validated for helium at pressures up to $1,000mbar$ and $T = 77K$. All measurements show a higher heat transfer coefficient than the model predicted, it is therefore fit for a conservative calculation.
- The convective cable cooling can be significantly increased with additional convection by solid–solid contact, e.g. placing the cable on the pipe floor instead of using spacers for centering.
- Furthermore, for a reliable thermal cable modelling, the thermal contact resistances of solid–solid interfaces need to be considered and were determined at $T = 77K$ for a single-phase cable sample. Yet further investigations are necessary.

When the findings are transferred to LH_2 environment, a simplified thermal model predicts sufficient cooling capacity of helium for a hybrid energy pipeline design with indirect cooling, considering steady-state. However, validations for LH_2 temperatures as well as cooling performance at transient fault events are still to be experimentally confirmed.

To compliment the technical design and investigation of a hybrid energy pipeline, the authors are conducting a techno-economic assessment in a case study targeting the transmission of 4 GW electrical power and up to 1.15 t/d LH_2 (publication submitted in 08–2025, [22,23]).

CRediT authorship contribution statement

Mira Wehr: Writing – original draft, Investigation, Formal analysis, Data curation. **Michael J. Wolf:** Writing – review & editing, Supervision, Investigation. **Tabea Arndt:** Writing – review & editing, Supervision, Project administration, Conceptualization.

Declaration of competing interest

The authors declare that they have no known competing financial interests or personal relationships that could have appeared to influence the work reported in this paper.

Acknowledgment

The authors thank all included persons at the Institute of Technical Physics (ITEP) that supported the conception and implementation of this work.

This work was carried out within the Hydrogen Flagship Project TransHyDE and was funded by the Federal Ministry of Education and Research under the funding grant number 03HY204A. The responsibility for the content of this publication lies with the author(s).

Appendix

List of abbreviations (not shown are variable indices which are explained in the text):

PTL	Power transfer line
LH_2	Liquid hydrogen
(2G) HTS	(2nd generation) high temperature superconductor
LN_2	Liquid nitrogen
MgB_2	Magnesium diboride
REBCO	Rare earth barium copper oxide
YBCO	Yttrium barium copper oxide
I_c	Critical current
w	Width
MLI	Multi-layer insulation
DC	Direct current
$\dot{Q}$	Heat transfer rate
λ	Thermal conductivity
L	Length
D, d	Diameter
T	Temperature
Pr	Prandtl number
Ra	Rayleigh number
g	Gravitational acceleration
β	Coefficient of thermal expansion
ν	Kinematic viscosity
α	Heat transfer coefficient
A	Area
U	Voltage
I	Current
PLA	Polylactic acid
PI	Polyimide
P	Power
R_{th}	Thermal resistance
δ_{PI}	Thickness PI foil
p_{He}	He pressure
$\bar{c}_p$	Mean heat capacity
$\dot{m}$	Mass flow

Data availability

Data will be made available on request.

References

[1] Lemmon, E.W., Bell, I.H., Huber, M.L., McLinden, M.O. NIST Standard Reference Database 23: Reference Fluid Thermodynamic and Transport Properties-REFPROP, Version 10.0, National Institute of Standards and Technology, Standard Reference Data Program, Gaithersburg, 2018.

[2] Grant PM. The Supercable: dual delivery of hydrogen and electric power. IEEE Trans Appl Supercond 2005;15(2):1810–3.

[3] Grant PM. Superconducting lines for the transmission of large amounts of electrical power over great distances: garwin–matisoo revisited forty years later. IEEE Trans Appl Supercond 2007;17(2):1641–7. https://doi.org/10.1109/TASC.2007.899981.

[4] Grant PM. Cryo-delivery Systems for the Co-transmission of Chemical and Electrical Power. AIP Conf Proc 2006;823(1):291–301. https://doi.org/10.1063/1.2202428.

[5] Kostyuk VV, et al. Experimental hybrid power transmission line with liquid hydrogen and mgb$_2$-based superconducting cable. Tech Phys Lett 2012;38(3):279–82. https://doi.org/10.1134/s106378501203025x.

[6] Vysotsky VS, et al. Cryogenic tests of 30 m flexible hybrid energy transfer line with liquid hydrogen and superconducting MgB_2 cable. Phys Procedia 2015;67:189–94. https://doi.org/10.1016/j.phpro.2015.06.033.

[7] Vysotsky VS, et al. Energy transfer with hydrogen and superconductivity – the review of the first experimental results. Phys Procedia 2015;65:299–302. https://doi.org/10.1016/j.phpro.2015.05.158.

[8] Vysotsky VS, et al. New 30-m flexible hybrid energy transfer line with liquid hydrogen and superconducting MgB_2 cable — development and test results. IEEE Trans Appl Supercond 2014;25(3):1–5. https://doi.org/10.1109/tasc.2014.2361635.
[9] Wimbush S, et al. A high-temperature superconducting (HTS) wire critical current database. figshare. Collection 2016. https://doi.org/10.6084/m9.figshare.c.2861821.v16.
[10] S. Yamaguchi et al., "Low Voltage and Large Current DC Superconducting Power Cable Designs for 10 km to 100 km Transmission Line Using Experimental Data of Ishikari Project", *Journal of Physics: Conference Series, 1293*(1), 2019, doi: 10.1088/1742-6596/1293/1/012067.
[11] Kottonau D, et al. Design comparisons of concentric three-phase HTS cables. IEEE Trans Appl Supercond 2019;29(6):1–8. https://doi.org/10.1109/tasc.2019.2897893.
[12] Lynch S. Hydrogen embrittlement phenomena and mechanisms. Corros Rev 2012;30(3–4):105–23. https://doi.org/10.1515/corrrev-2012-0502.
[13] Qiu Y, et al. Research progress of cryogenic materials for storage and transportation of liquid hydrogen. Metals 2021;11(7):1101. https://doi.org/10.3390/met11071101.
[14] Dortman G, et al. Hydrogenation of thin Y-Ba-Cu-O films: electrical transport and structure properties of YBa2Cu3O7 and YBa2Cu4O8. Phys Rev B 1994;49:600–6. https://doi.org/10.1103/PhysRevB.49.600.
[15] Shah D, et al. Cryogenic thermal modeling and experimental validation of novel heat sink for helium gas cooled superconducting devices. IEEE Trans Appl Supercond 2014;25(3):1–4.
[16] Van Der Laan DC, et al. Development of CORC® cables for helium gas cooled power transmission and fault current limiting applications. Supercond Sci Technol 2018;31(8):085011.
[17] Suttell, Nick, et al. "Thermal modeling of gaseous helium as a cryogen for high temperature superconducting cable components." *IEEE transactions on applied superconductivity* 25.3 (2014): 1-5.
[18] M. N. Özisik, "Heat Transfer – A Basic Approach", p. 468-475, 1985.
[19] Liu C. Natural convection heat transfer in long horizontal cylindrical annuli. Int Develop Heat Transf 1967;117:976–84.
[20] Marquardt ED, et al. Cryogenic material properties database. Cryocoolers 2002;11:681–7.
[21] Bagrets N, et al. Thermal resistance between metallic surfaces of copper and stainless steel at different temperatures and applied forces for high current HTS cable-in-conduit conductors. IEEE Trans Appl Supercond 2022;32(6):1–5. https://doi.org/10.1109/TASC.2022.3154327.
[22] S. Palacios et al., "AppLHy! und TransHyDE – Hybride Pipeline: Synergetische Energieübertragung mittels HTS und LH_2", *oral presentation at ZIEHL IX conference (Berlin 04-2024)*, url: https://publikationen.bibliothek.kit.edu/1000173137.
[23] S. Palacios et al., „Combined Energy Transmission by LH_2 and HTS: Study of a Hybrid Pipeline", *poster presentation at 16th EUCAS conference (Bologna 09-2023)*, doi: 10.13140/RG.2.2.10355.75046.